# Local Density Functional Study of Oxoiron(IV) Porphyrin Complexes and Their One-Electron Oxidized Derivatives. Axial Ligand Effects

**Jens Antony, Michael Grodzicki, and Alfred X. Trautwein***

*Institut für Physik, Medizinische Universität zu Lübeck, Ratzeburger Allee 160, D-23538 Lübeck, Germany*

*Received: October 22, 1996*[⊗]

A systematic study of the electronic structure of models for the active sites of heme enzymes such as peroxidases and cytochromes P450 has been carried out for high-valent transition states of their catalytic cycles, namely, compound I and compound II for peroxidases, as a function of the second axial ligand. The investigation is based on molecular orbital calculations in local density approximation and comprises five-coordinated oxoiron(IV) porphyrin as well as the corresponding six-coordinated species with chlorine, imidazole, and $H_3CS^-$ as axial ligands. In all cases, the ground state of compound II is obtained as the ferryl $(t_{2g})^4$ configuration $(3d_{xy})^2(3d_{xz},3d_{xy})^2$ with total spin $S = 1$ distributed between the iron and oxygen atom in a ratio of approximately 60/40. Different electronic states of compound I with the radical located in the $a_{1u}$ or $a_{2u}$ orbitals of the porphyrin or in the lone-pair orbital of the axial ligand are discussed in detail. The corresponding Heisenberg exchange coupling constants $J$ between the oxoiron and the radical spin are calculated, and the influence of the position and orientation of the axial ligand on $J$ is investigated. The results are correlated with the available experimental data.

## I. Introduction

High-valent oxoiron(IV) porphyrins are involved as the active sites in reactions catalyzed by heme enzymes such as peroxidases[1] and cytochromes P450.[2] Two reaction intermediates, denoted for peroxidases as compound II and compound I, have been identified that are one and two oxidation equivalents, respectively, above the ferric resting state. Differences in chemical specificity in peroxidase- and P450-based reactions are commonly ascribed to different second axial ligands. In order to explore such differences, synthetic oxoiron(IV) porphyrins and their corresponding cation radical systems have been investigated by various spectroscopic techniques including X-ray crystallography and EXAFS,[3,4] EPR and Mössbauer spectroscopy,[5−13] NMR and magnetic susceptometry,[14−19] electronic absorption,[20−22] resonance Raman,[23−26] and ENDOR.[27−29] However, conclusive evidence for correlations between reactivity and electronic properties of the heme group, e.g., the Fe═O bond strength or the spin density at the oxogroup, has not yet been obtained.[18]

The majority of theoretical investigations on the quantum chemical level has been restricted to semiempirical methods such as iterative extended Hückel[30,31] and INDO calculations.[32,33] Hartree−Fock (HF) based approaches for open-shell transition metal complexes like the compound I and compound II analogues would require inclusion of at least some correlation in order to obtain qualitatively correct results. This has been demonstrated by comparative calculations on the open-shell HF and complete active space self-consistent field (CASSCF) levels, respectively.[34,35] In the HF calculation of the compound II analogue the two unpaired spins are almost completely located at the iron (1.91) with negligible delocalization toward the oxogroup (0.06), while the CASSCF calculation yields a distribution of 1.17 and 0.82, respectively, in accordance with results of ENDOR measurements.[28]

Attractive alternatives to calculations of this type are methods based on density functional theory (DFT),[36−38] which have been proven particularly useful during the last decade, since they can reliably handle even large transition metal complexes without a prohibitive amount of computing time and memory space so that such an approach offers the opportunity of systematic theoretical studies on high-valent oxoiron porphyrins. The first attempt in this direction has been a spin-restricted scattered wave Xα calculation on a six-coordinated model of the active site of compound I and compound II of horseradish peroxidase (HRP) with pyridine as second axial ligand.[39] Very recently, a DFT calculation in local density approximation (LDA) has appeared dealing with a model of compound I and compound II, however, without any second axial ligand.[40] A systematic study of the influence of axial ligation and terminal substituents in compound I and compound II model analogues based on the local density approximation has not yet been published to our knowledge.

This work presents a theoretical study of the electronic structure of high-valent compound I and compound II analogues by molecular orbital (MO) calculations within the local density approximation to determine (i) the molecular orbitals of compound II and compound I, (ii) the site of oxidation in compound II that yields compound I, (iii) the mode and strength of exchange coupling between the radical ($S' = 1/2$) and the oxoiron ($S = 1$) spin, and (iv) the influence of the second axial ligand on (i)−(iii).

In a subsequent paper,[41] the effect of terminal substituents at the porphyrin ring will be examined.

## II. Geometrical and Computational Assumptions

The reference model system for the subsequent investigations on high-valent oxoiron porphyrins consists of a planar porphyrin macrocycle with symmetry $D_{4h}$, hydrogen atoms as peripheral substitutents, and $Cl^-$ as the second axial ligand. The porphyrin plane coincides with the *xy*-plane, and the nitrogen atoms are located on the coordinate axes. The atomic positions are derived from crystal structure data of free base porphine[42] by taking the average values of equivalent bond distances and bond angles (Table 1) in order to preserve the 4-fold symmetry of the porphyrin core. Carbon−hydrogen bond lengths are set to 1.09

* To whom correspondence should be addressed. Telephone: +49-451-500-4200. Fax: +49-451-500-4214. E-mail trautwein@physik.mu-luebeck.de.

⊗ Abstract published in *Advance ACS Abstracts,* March 1, 1997.

S1089-5639(96)03295-1 CCC: $14.00 

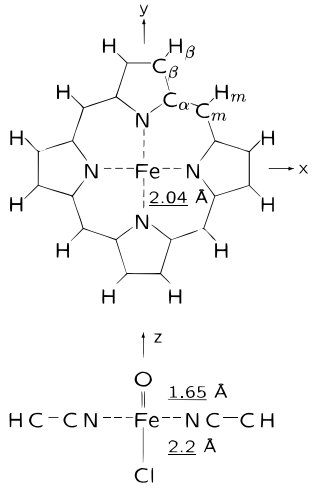


**Figure 1.** Geometry of the reference model system with planar $D_{4h}$ porphyrin macrocycle. The molecule is oriented paralled to the *xy*-plane with the nitrogen atoms on the coordinate axes. A single oxygen in the positive and chlorine in the negative *z* direction act as first and second axial ligands, respectively.

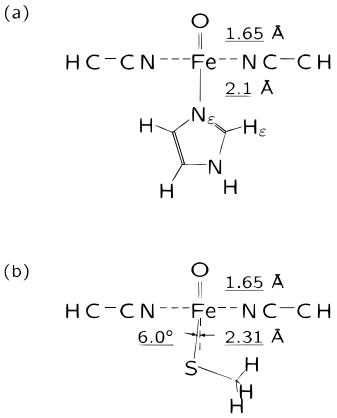


**Figure 2.** Variation of the axial ligand: (a) model for the histidine residue; (b) model for the cysteinate residue.

**TABLE 1: Bond Distances and Bond Angles for a Planar $D_{4h}$ Porphyrin Macrocycle Derived from the Crystal Structure Data of Free Base Porphine[42] by Taking the Average Values of Equivalent Bond Distances and Bond Angles**

| *d* | Å | *θ* | deg |
|---|---|---|---|
| N−$C_\alpha$ | 1.38 | $C_\alpha$−N−$C_\alpha'$ | 107.3 |
| $C_\alpha$−$C_\beta$ | 1.44 | N−$C_\alpha$−$C_\beta$ | 108.9 |
| $C_\beta$−$C_\beta'$ | 1.36 | $C_\alpha$−$C_\beta$−$C_\beta'$ | 107.5 |
| $C_\alpha$−$C_m$ | 1.38 | N−$C_\alpha$−$C_m$ | 125.1 |

Å. The iron is placed at the center of the porphyrin ring, resulting in an iron−nitrogen distance of 2.04 Å. The oxoiron distance is assumed to be 1.65 Å, consistent with structural data derived from EXAFS[4,43] and X-ray[3] measurements for high-valent oxoiron(IV) porphyrin systems. The distance between the chlorine anion and the iron is taken as 2.2 Å (Figure 1). The symmetry of this reference system is $C_{4v}$.

Replacing the axial ligand by imidazole or $H_3CS^-$ aims at modeling the histidine and cysteinate residues coordinating the active center in peroxidases and cytochromes P450. The geometrical data of imidazole are taken from the free molecule[44] (Figure 2a). The plane through imidazole is perpendicular to the porphyrin plane and contains two opposite methine carbon atoms of the porphyrin ring. This orientation is obtained as the minimum of the total energy when rotating imidazole around the *z* axis. The pyridine-like nitrogen atom $N_\epsilon$ and the center-of-mass of the imidazole are placed on the *z* axis with a distance

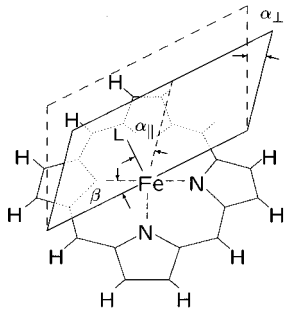


**Figure 3.** Geometrical variation of the axial ligand. The axial ligand is rigid, and the angle between the iron atom in the porphyrin center (Fe), the coordinating atom (L), and any other atom of the ligand remains constant.

$d$(Fe−$N_\epsilon$) of 2.1 Å. The geometry and orientation of the $H_3CS^-$ anion (Figure 2b) are taken from the crystal structure of the hemoprotein domain of P450BM−3[45] with the iron−sulfur distance set to 2.31 Å. The angle between the iron, sulfur, and carbon is 104.5°, and the axis through the iron and sulfur is tilted by an angle of $\alpha = 6°$ out of the porphyrin normal direction (*z* axis). The plane through the iron, sulfur, and carbon intersects the porphyrin plane at an angle of $\beta = 107.3°$ with respect to the *x* axis (see also Figure 3).

Starting with these reference geometries, the position of the axial ligands may be varied in order to investigate the influence of their orientation on the electronic structure of the heme group. Assuming the axial ligands as rigid, their position relative to the porphyrin core is determined by six geometrical degrees of freedom. Assuming further that the angle between the iron, the coordinating axial ligand atom ($N_\epsilon$ or S), and any other atom of the ligand remains constant, the number of degrees of freedom is reduced to four, viz., the bond distance *d* of the axial ligand, rotation of the axial ligand around the *z* axis (rotation angle $\beta$), tilting of the ligand within the ligand plane (tilting angle $\alpha_\parallel$), and tilting the ligand plane (tilting angle $\alpha_\perp$). The total tilting angle $\alpha$ is given by the relation $\cos\alpha = \cos\alpha_\parallel \cos\alpha_\perp$. Figure 3 displays these geometrical degrees of freedom of the axial ligands. Possible deformations of the porphyrin core due to interactions with the axial ligands are neglected throughout.

The molecular orbital calculations presented here have been performed within the local density approximation[36−38] by the self-consistent charge (SCC)-X$\alpha$ method.[46] This approach is based on a model potential for the valence electron density that enables the analytical evaluation of all angular parts of the matrix elements and leaves only one-dimensional numerical integrations for the exchange−correlation potential. The population analysis is performed by numerical integration of the electron density within appropriately chosen atomic spheres. As a whole, the SCC-X$\alpha$ code is an order of magnitude faster than the X$\alpha$ option of GAUSSIAN94 and requires substantially less memory space. For these reasons this method is particularly suited for describing the electronic properties of large molecules containing transition metal atoms as shown by several applications to systems of biological relevance[47−49] and other transition metal compounds.[50−52]

## III. Results

**A. Electronic Structure of Compound II.** A spin-restricted MO calculation on the reference model system with $Cl^-$ as an axial ligand reveals the characteristic pattern of the Fe(3d) orbitals for an approximately octahedral coordination, viz., the splitting into the $t_{2g}$-type (Figure 4) and $e_g$-type manifolds. The $3d_{x^2-y^2}$ and $3d_{z^2}$ orbitals of the iron are separated from the $3d_{xz}$, $3d_{yz}$ orbitals by 0.80 and 2.04 eV because of the strong $\sigma$

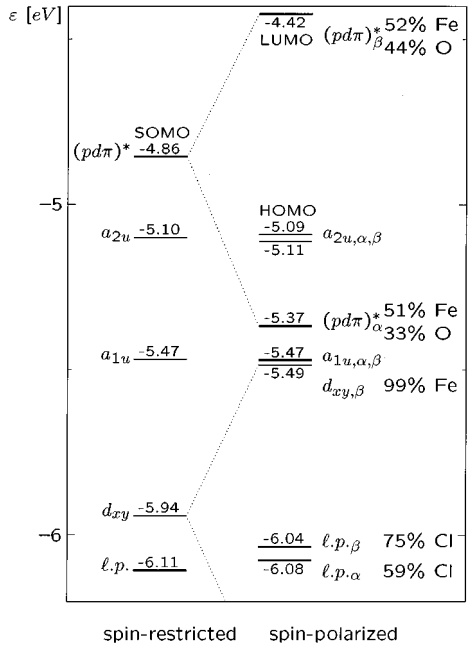


**Figure 4.** Orbital energies between −4.4 and −6.2 eV in the ground state of six-coordinated oxoiron (IV) porphyrin with a chlorine anion as the axial ligand obtained by a spin-restricted and a spin-polarized MO calculation. Behind the MO's the character of the wave functions is displayed (l.p., lone-pair orbital of the axial ligand; α, spin up; $\beta$, spin down; (pd$\pi$)* denotes the $\pi$ antibonding combination of Fe($3d_{xz}$, $3d_{yz}$) and O($2p_x$, $2p_y$) orbitals).

interaction with the in-plane nitrogen lone-pair orbitals of the porphyrin core and the $p_z$ atomic orbitals (AO's) of the axial ligands, respectively. The Fe(3d) character of these MO's amounts to 62% and 52%. The $t_{2g}$-type orbitals are split into $3d_{xy}$ and into the degenerate $3d_{xz}$, $3d_{yz}$ orbitals denoted as $3d_\pi$. These orbitals together with the three highest occupied ligand MO's are shown in the left part of Figure 4. The $3d_{xy}$ orbital is a pure iron 3*d* orbital with 99% iron character. The Fe($3d_\pi$) orbitals undergo strong $\pi$ interactions with the $2p_x$ and $2p_y$ orbitals of the oxygen atom. The resulting 2-fold degenerate antibonding MO, denoted as (pd$\pi$)*, reveals appreciable O(2p) admixture of 42% and constitutes the highest occupied MO (HOMO) containing two electrons so that each orbital is singly occupied and is denoted as SOMO in Figure 4. The two porphyrin MO's, $a_{1u}$ and $a_{2u}$ in the notation of $D_{4h}$ symmetry are linear combinations of the out-of-plane $p_z$ orbitals of the carbon and nitrogen atoms. The $a_{1u}$ orbital, with main amplitudes at the pyrroline carbon atoms, is 0.38 eV below the $a_{2u}$, with main amplitudes at the nitrogens and the methine carbons. Approximately 1 eV below the $a_{2u}$ is a MO with 70% participation of chlorine $3p_x$ and $3p_y$ AO's, which will be denoted as the axial ligand lone-pair (l.p.) orbital. Filling the MO's according to the Pauli principle and Hund's rule results in a triplet ground state ($S = 1$) with the $(t_{2g})^4$ configuration $(3d_{xy})^2$ $(3d_{xz})^1$ $(3d_{xy})^1$ of iron. Thus, the MO calculation yields the ferryl state Fe(IV) as the ground state, in accordance with Mössbauer spectroscopic results obtained on high-valent intermediates of peroxidase[5−7] and biomimetic model complexes.[8−12]

Because the resulting ground state corresponds to an open-shell configuration, a spin-polarized calculation is necessary in order to obtain a more detailed picture. The correlation between the spin-restricted and the spin-polarized MO calculation is displayed in Figure 4. The iron 3d orbitals split into majority (spin up, α) and minority spin (spin down, $\beta$) orbitals as a consequence of the exchange interaction. Usually, the size of this exchange splitting becomes larger with increasing 3d character of the molecular orbital, and amounts to 0.69 eV for the $3d_{z^2}$, 0.62 eV for the $3d_{x^2-y^2}$ (both not shown in Figure 4), 0.94 eV for the $3d_\pi$, and 0.92 eV for the $3d_{xy}$ orbital (Table 2). The reason for the slightly larger exchange splitting in $3d_\pi$ is a different covalent interaction between Fe and O for the α and $\beta$ spin orbitals. This is reflected in the participation of O(2p) by 44% in the $\beta$ spin orbital vs 33% O(2p) in the α spin orbital, the latter being slightly delocalized toward the chlorine anion with 14% contribution of the Cl($3p_x$, $p_y$). Correspondingly, the Cl(3p) lone-pair α and $\beta$ MO's exhibit considerably different Cl(3p) participation, 59% and 75%, respectively. Owing to the exchange splitting of the Fe(3d) orbitals, the HOMO is now the $a_{2u}$ orbital of the porphyrin core, while the lowest unoccupied MO (LUMO) is the $(pd\pi)^*_\beta$ spin orbital (cf. Figure 4) with a HOMO/LUMO gap of 0.67 eV. The two unpaired electrons occupying the $(pd\pi)^*_\alpha$ spin orbitals give rise to the system spin $S = 1$ being almost completely localized within the Fe═O moiety. The corresponding singlet state is calculated with 0.35 eV above the triplet state, in accordance with Hund's rule.

**TABLE 2: Orbital energies ϵ in eV for the HOMO's and LUMO's in the Ground States of Compound II and Compound I of Five- (O═FeP) and Six-Coordinated Oxoiron(IV) Porphyrins with a Chlorine Anion ($Cl^-$), Imidazole (Imi), and $SCH_3^-$ as Second Axial Ligands (cf. Figures 4 and 5)**

| | O═FeP | | $Cl^-$ | | Imi | | $H_3CS^-$ | |
|---|---|---|---|---|---|---|---|---|
| MO[a] | cpd II | cpd I | cpd II | cpd I | cpd II | cpd I | cpd II | cpd I |
| $d_{z^2,\alpha}$ | −6.64 | −9.17 | −3.16 | −5.31 | −5.19 | −7.28 | −2.65 | −5.43 |
| $d_{z^2,\beta}$ | −5.84 | −8.36 | −2.47 | −4.61 | −4.44 | −6.54 | −1.96 | −4.64 |
| $d_{z^2-y^2,\alpha}$ | −6.95 | −9.39 | −4.36 | −6.66 | −6.10 | −8.33 | −4.08 | −6.46 |
| $d_{z^2-y^2,\beta}$ | −6.34 | −8.77 | −3.74 | −6.00 | −5.51 | −7.69 | −3.41 | −5.85 |
| $(pd\pi)^*_{\parallel,\alpha}$ | −8.28 | −10.85 | −5.37 | −7.70 | −7.52 | −9.77 | −4.94 | −7.76 |
| $(pd\pi)^*_{\parallel,\beta}$ | −7.24 | −9.83 | −4.42 | −6.75 | −6.52 | −8.78 | −3.95 | −6.75 |
| $(pd\pi)^*_{\perp,\alpha}$ | −8.28 | −10.85 | −5.37 | −7.70 | −7.52 | −9.77 | −5.02 | −7.73 |
| $(pd\pi)^*_{\perp,\beta}$ | −7.24 | −9.83 | −4.42 | −6.75 | −6.52 | −8.78 | −3.86 | −6.73 |
| $d_{xy,\alpha}$ | −9.37 | −12.06 | −6.41 | −8.87 | −8.62 | −10.99 | −6.05 | −8.85 |
| $d_{xy,\beta}$ | −8.37 | −11.11 | −5.49 | −7.97 | −7.67 | −10.07 | −5.07 | −7.92 |
| $a_{2u,\alpha}$ | −7.71 | −10.61 | −5.09 | −7.98 | −6.99 | −9.88 | −4.80 | −7.27 |
| $a_{2u,\beta}$ | −7.68 | −10.39 | −5.11 | −7.78 | −7.01 | −9.68 | −4.80 | −7.25 |
| $a_{1u,\alpha}$ | −7.78 | −10.37 | −5.47 | −8.03 | −7.31 | −9.85 | −5.35 | −7.63 |
| $a_{1u,\beta}$ | −7.77 | −10.40 | −5.47 | −8.07 | −7.31 | −9.89 | −5.35 | −7.63 |
| $l.p._{\perp,\alpha}$ | | | −6.08 | −8.64 | −11.37 | −13.45 | −4.38 | −9.25 |
| $l.p._{\perp,\beta}$ | | | −6.04 | −8.55 | −11.35 | −13.23 | −4.53 | −8.37 |
| $l.p._{\parallel,\alpha}$ | | | −6.08 | −8.64 | −11.66 | −14.03 | −5.96 | −10.44 |
| $l.p._{\parallel,\beta}$ | | | −6.04 | −8.55 | −11.55 | −13.83 | −5.79 | −9.83 |

[a] l.p., lone-pair orbital of the axial ligand; α, spin up; $\beta$, spin down; (pd$\pi$)* denotes the $\pi$ antibonding combination of Fe($3d_{xz}$,$d_{xy}$) and O($2p_x$, $p_y$) orbitals.

Next, the changes of the orbital energies of interest with respect to different axial ligands are considered (Figure 5). In order to facilitate the comparison, the orbital energies are referenced to the energy of the $a_{1u}$ MO. Removing the chlorine anion does not change the symmetry of the complex from $C_{4v}$, while replacing the chlorine anion by imidazole or $H_3CS^-$ reduces the symmetry to $C_s$ or $C_1$, respectively. The fictitious case of a five-coordinated iron with iron left in the porphyrin plane is shown for comparison on the left side of Figure 5. The main changes caused by removing the chlorine anion concern the stabilization of the porphyrin $a_{2u}$ orbital and of the MO's with mainly Fe(3d) character relative to $a_{1u}$, which is especially pronounced for the $3d_{z^2}$ orbital because of the lack of $\sigma$ interaction with the Cl($3p_z$) orbital, leading to an increase of the Fe(3d) character. The missing $\pi$ interaction of the Cl($3p_x$, $3p_y$) orbitals with the (pd$\pi$)* orbital enhances mainly the O(2p) contribution of the $(pd\pi)^*_\alpha$ orbital, while the character of the $(pd\pi)^*_\beta$ orbital is virtually unaffected.

In the case of imidazole-ligated porphyrin, the main features of the $\sigma$-type MO's with mainly Fe(3d) character are similar to the chlorine-ligated porphyrin. In spite of the reduced sym-

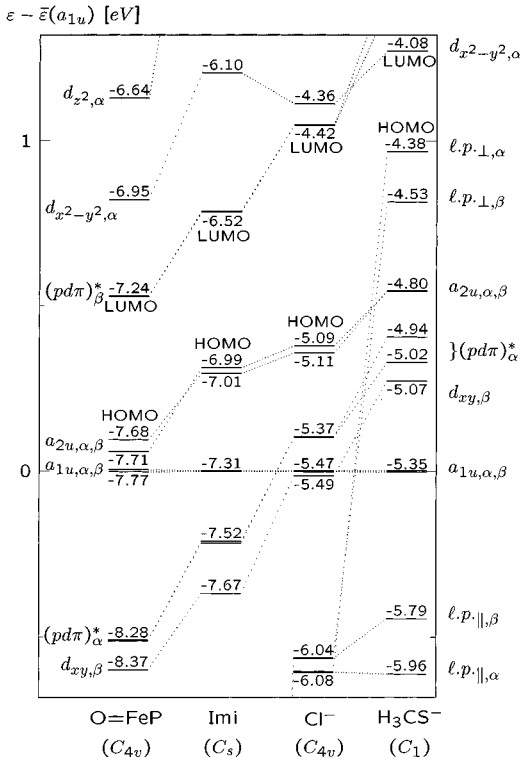


**Figure 5.** Correlation diagram for the orbital energies of the HOMO's and LUMO's of five- (O═FeP) and six-coordinated oxoiron (IV) porphyrins with a chlorine anion ($Cl^-$), an imidazole molecule (Imi), and an $H_3CS^-$ anion as axial ligands. The energies are given relative to the orbital energy of the $a_{1u}$ MO $\bar{\epsilon}(a_{1u}) = (\epsilon(a_{1u,\alpha}) + \epsilon(a_{1u,\beta}))/2$; $\epsilon$-$(a_{1u}) = -7.77$ eV for O═FeP, $-5.47$ eV for $Cl^-$, $-7.31$ eV for Imi, and $-5.35$ eV for $H_3CS^-$.

metry, the (pd$\pi$)* MOs remain almost degenerate, with a splitting of less than 0.01 eV and negligible contribution from the pyridine-like nitrogen atom, indicating that there is virtually no $\pi$ interaction between iron and $N_\epsilon$. Consequently, the character of this orbital compares well with the five-coordinated oxoiron(IV) porphyrin (Table 3). The reason is the large energy separation between the Fe(3d) and the $N_\epsilon$(2p) AO's, so that the corresponding MO's with $N_\epsilon$(2p) character are more than 4 eV below the $a_{1u}$ and $a_{2u}$ orbitals. The $a_{2u}$ is the HOMO for the five-coordinated oxoiron(IV) porphyrin and for six-coordinated oxoiron(IV) porphyrin with imidazole and chlorine as axial ligands. The $a_{1u}$ orbital is 0.09, 0.31, and 0.38 eV lower in energy, respectively. The LUMO is the $(pd\pi)^*_\beta$ orbital with 0.43, 0.47, and 0.67 eV above the HOMO. Because of this similarity in the one-electron energy structure near the occupation border, the ground state is the same spin triplet state in all three cases.

With $H_3CS^-$ as the axial ligand, the pattern of the molecular orbital energies of the oxoiron(IV) porphyrin exhibits considerable differences. First, the HOMO becomes a predominantly sulfur 3p orbital with orientation perpendicular to the plane defined by the iron, sulfur, and carbon of the $H_3CS^-$ group. The sulfur 3p contribution to this orbital amounts to 71% ($\alpha$) and 73% ($\beta$) and will thus be denoted as the S(3p) lone-pair (l.p.$_\perp$) orbital. It is separated by 0.42 eV for the $\alpha$ and 0.27 eV for the $\beta$ spin orbital from the $a_{2u}$ orbital. The MO's with S(3p) in-plane character are $-1.57$ eV ($\alpha$) and $-1.41$ eV ($\beta$) below the HOMO. The $a_{1u}/a_{2u}$ splitting increases to 0.55 eV because of S(3p) admixture of about 15% to the $a_{2u}$. The $(pd\pi)^*_\alpha$ MO is split by about 0.1 eV into the out-of-plane $(pd\pi)^*_{\perp,\alpha}$ and the in-plane $(pd\pi)^*_{\parallel,\alpha}$ orbitals because of different $\pi$ interactions with the sulfur 3p AO's perpendicular and parallel to the Fe−S−C plane. Correspondingly, the $(pd\pi)^*_{\perp,\alpha}$ orbital contains contributions from S(3p) at 9% and O(2p) at 40%, similar as in case of the chlorine-ligated porphyrin. In contrast, the $(pd\pi)^*_{\parallel,\alpha}$ orbital has negligible amplitude at the sulfur atom and does not change its composition compared with the five-coordinated and the imidazole-coordinated oxoiron(IV) porphyrin. Similar conclusions apply to the corresponding unoccupied $(pd\pi)^*_\beta$ orbital, not shown in Figure 5. Finally, the crystal field splitting is smaller than the exchange splitting of the individual Fe(3d) orbitals because the $t_{2g}$-type molecular orbitals are destabilized by the axial ligands, whereas the $3d_{x^2-y^2}$ orbitals remain comparatively unaffected (Figure 5), and the $3d_{x^2-y^2,\alpha}$ orbital becomes the LUMO with 0.3 eV above the HOMO.

**TABLE 3: Percentage Contribution of the 2p AO's at the Nitrogen (%N), Carbon (%C), and Oxygen (%O) Atoms, the 3p AO's at the Chlorine (%Cl) and Sulfur (%S) Atoms, and the 3d AO's at the Iron Atom (%Fe) to the Relevant MO's of Compound II and Compound I[b]**

| | | O═FeP | | $Cl^-$ | | Imi | | $H_3CS^-$ | | |
|---|---|---|---|---|---|---|---|---|---|---|
| MO | % | cpd II | cpd I | cpd II | cpd I | cpd II | cpd I | cpd II | cpd I | |
| $(pd\pi)^*_{\parallel,\alpha}$ | L | | | 13.6 | 9.9 | 0.0 | 0.0 | 0.0 | 0.1 | |
| | O | 40.5 | 40.1 | 33.3 | 34.8 | 40.0 | 39.8 | 42.3 | 40.0 | |
| | Fe | 54.7 | 55.2 | 51.4 | 53.8 | 55.6 | 56.3 | 53.5 | 55.8 | |
| $(pd\pi)^*_{\parallel,\beta}$ | L | | | 2.9 | 2.8 | 0.0 | 0.0 | 0.1 | 0.0 | |
| | O | 43.9 | 44.3 | 43.7 | 43.3 | 43.6 | 43.7 | 44.8 | 43.9 | |
| | Fe | 53.0 | 52.5 | 51.6 | 52.1 | 53.4 | 53.2 | 52.8 | 53.1 | |
| $(pd\pi)^*_{\perp,\alpha}$ | L | | | 13.6 | 9.9 | 0.0 | 0.0 | 9.0 | 2.3 | |
| | O | 40.5 | 40.1 | 33.3 | 34.8 | 39.9 | 39.6 | 40.1 | 38.3 | |
| | Fe | 54.7 | 55.2 | 51.4 | 53.8 | 55.6 | 56.3 | 43.6 | 56.5 | |
| $(pd\pi)^*_{\perp,\beta}$ | L | | | 2.9 | 2.8 | 0.0 | 0.0 | 10.7 | 1.7 | |
| | O | 43.9 | 44.3 | 43.7 | 43.3 | 43.4 | 43.5 | 36.1 | 42.1 | |
| | Fe | 53.0 | 52.5 | 51.6 | 52.1 | 53.3 | 53.2 | 51.2 | 54.1 | |
| $a_{2u,\alpha}$ | N | 29.5 | 28.7 | 42.5 | 41.3 | 39.0 | 37.6 | 38.3 | 39.8 | |
| | $C_m$ | 49.3 | 54.8 | 51.6 | 51.8 | 54.0 | 55.3 | 42.4 | 52.7 | |
| | L | | | 3.2 | 3.9 | 1.5 | 1.7 | 12.7 | 2.9 | |
| $a_{2u,\beta}$ | N | 33.9 | 31.8 | 42.1 | 41.5 | 38.9 | 38.1 | 36.7 | 39.8 | |
| | $C_m$ | 54.9 | 55.9 | 51.2 | 51.0 | 54.3 | 54.6 | 39.9 | 51.8 | |
| | L | | | 3.7 | 4.1 | 1.3 | 1.5 | 18.3 | 4.0 | |
| $a_{1u,\alpha}$ | $C_\alpha$ | 78.6 | 79.8 | 76.7 | 78.5 | 77.9 | 79.2 | 76.5 | 77.6 | |
| | $C_\beta$ | 21.4 | 20.2 | 23.3 | 21.5 | 22.1 | 20.7 | 23.3 | 22.2 | |
| $a_{1u,\beta}$ | $C_\alpha$ | 78.5 | 80.2 | 76.6 | 79.0 | 77.8 | 79.7 | 76.4 | 77.7 | |
| | $C_\beta$ | 21.5 | 19.8 | 23.4 | 21.0 | 22.1 | 20.3 | 23.4 | 22.1 | |
| l.p.$_{\perp,\alpha}$ | L | | | 59.5 | 65.9 | 27.8 | 30.3 | 71.1 | 41.6[a] | |
| | O | | | 7.5 | 6.2 | 4.0 | 12.8 | 3.2 | 10.0 | |
| | Fe | | | 4.5 | 2.4 | 0.0 | 11.2 | 13.3 | 3.8 | |
| l.p.$_{\perp,\beta}$ | L | | | 74.9 | 74.2 | 33.6 | 28.5 | 72.8 | 66.9 | |
| | O | | | 8.4 | 9.7 | 0.6 | 6.0 | 9.7 | 1.7 | |
| | Fe | | | 1.0 | 1.6 | 0.1 | 3.3 | 2.5 | 0.2 | |

[a] The reduction of S(3*p*) character after ionization is caused by mixing with occupied porphyrin $\pi$-orbitals, which contain the missing 30% S amplitude, leading to 17.5% N, 2.4% $C_\alpha$, 16.5% $C_\beta$, and 1.4% $C_m$ contribution to l.p.$_{\perp,\alpha}$ in compound I. [b] L denotes the coordinating atom of the axial ligand; L = Cl, $N_\epsilon$, or S.

Table 4 displays the charge (in units of e) and spin (in units of $\hbar/2$) distributions of the four systems under study. The charge density within the porphyrin macrocycle is essentially insensitive to axial coordination. The pyrroline nitrogen atoms are always negatively charged with an average effective charge between $-0.21$ and $-0.24$. All carbon atoms are nearly neutral. The effective charge of the iron in five-coordinated oxoiron(IV) porphyrin is 0.93, while the oxygen has a negative charge of $-0.47$. Addition of the axial ligand slightly increases the polarity of the Fe═O bond, with the effective charge of iron ranging from 0.96 to 0.98 and that of oxygen from $-0.51$ to $-0.59$. The overlap population, indicating the covalent bond strength, is 0.203 for the Fe−N and 0.524 for the Fe═O bond in five-coordinated oxoiron(IV) porphyrin (Table 4). These values are lowered by merely 5% for Fe═O and by 10% for Fe−N when the anionic ligands $Cl^-$ and $H_3CS^-$ are coordinated, whereas addition of imidazole does not show any appreciable effect.

**TABLE 4: Effective Atomic Charges $Q$ (in units of e), Spin Densities $\sigma$ (in units of $\hbar/2$), and Overlap Population (in e) for the Ground States of Compound II and Compound I**

| | | O═FeP | | $Cl^-$ | | Imi[a] | | $H_3CS^-$ [a] | |
|---|---|---|---|---|---|---|---|---|---|
| atom | | cpd II | cpd I | cpd II | cpd I | cpd II | cpd I | cpd II | cpd I |
| N | $Q$ | −0.21 | −0.17 | −0.22 | −0.17 | −0.22 | −0.17 | −0.23 | −0.20 |
| | $\sigma$ | −0.036 | −0.104 | −0.029 | 0.097 | −0.022 | 0.090 | −0.030 | 0.012[b] |
| $C_\alpha$ | $Q$ | 0.02 | 0.05 | 0.02 | 0.05 | 0.02 | 0.05 | 0.02 | 0.03 |
| | $\sigma$ | 0.004 | 0.017 | 0.003 | −0.022 | 0.002 | −0.018 | 0.003 | 0.013 |
| $C_\beta$ | $Q$ | 0.01 | 0.02 | 0.00 | 0.01 | 0.00 | 0.01 | 0.00 | 0.01 |
| | $\sigma$ | −0.001 | −0.016 | −0.001 | 0.000 | −0.001 | 0.003 | −0.001 | 0.015 |
| $C_m$ | $Q$ | 0.04 | 0.08 | 0.04 | 0.08 | 0.03 | 0.08 | 0.04 | 0.04 |
| | $\sigma$ | −0.018 | −0.183 | −0.001 | 0.175 | −0.001 | 0.179 | −0.001 | −0.001 |
| L | $Q$ | | | −0.57 | −0.53 | −0.21 | −0.19 | −0.41 | −0.14 |
| | $\sigma$ | | | 0.020 | 0.059 | −0.018 | −0.002 | 0.022 | 0.697 |
| O | $Q$ | −0.47 | −0.42 | −0.54 | −0.51 | −0.51 | −0.48 | −0.59 | −0.51 |
| | $\sigma$ | 0.934 | 0.933 | 0.934 | 0.932 | 0.914 | 0.920 | 0.866 | 0.922 |
| Fe | Q | 0.93 | 0.90 | 0.96 | 0.89 | 0.98 | 0.89 | 0.98 | 0.94 |
| | $\sigma$ | 1.253 | 1.124 | 1.154 | 1.128 | 1.187 | 1.152 | 1.213 | 1.176 |

| | O═FeP | | $Cl^-$ | | Imi[a] | | $H_3CS^-$ [a] | |
|---|---|---|---|---|---|---|---|---|
| bond | cpd II | cpd I | cpd II | cpd I | cpd II | cpd I | cpd II | cpd I |
| Fe−N | 0.203 | 0.218 | 0.178 | 0.192 | 0.198 | 0.212 | 0.170 | 0.195 |
| Fe−L | | | 0.206 | 0.217 | 0.131 | 0.159 | 0.156 | 0.135 |
| Fe═O | 0.524 | 0.548 | 0.500 | 0.526 | 0.527 | 0.548 | 0.518 | 0.535 |

[a] Average values are given for the atoms of the porphyrin macrocycle and for Fe−N. [b] The spin density at the pyrroline nitrogen atoms exhibits a distinct anisotropy: $\sigma$ (N,+$x$) = 0.067, $\sigma$ (N,+$y$) = −0.020, $\sigma$ (N,−$x$) = 0.015, $\sigma$ (N,−$y$) = −0.012.

The spin density in five-coordinated oxoiron(IV) porphyrin is almost completely localized within the oxoiron(IV) subunit (Table 4) and amounts to 1.253 for iron and 0.934 for oxygen so that the total spin of the oxoiron(IV) subunit slightly exceeds 2. The excess spin is compensated by a small negative spin density (−0.036) at each nitrogen of the macrocycle because of different $\sigma$ interactions of the $3d_{x^2-y^2,\alpha}$ and $3d_{x^2-y^2,\beta}$ orbitals with the nitrogens and a small negative spin density (−0.018) at the methine carbon atoms. Addition of the axial ligand leads to a reduction of the excess spin density at the oxoiron(IV) subunit and of the negative spin density at the porphyrin macrocycle so that the methine carbon atoms are almost diamagnetic in the six-coordinated oxoiron(IV) porphyrins. Owing to the Cl(3p) and S(3p) contribution to the $(pd\pi)^*_\alpha$ orbital, the spin density of the oxoiron(IV) porphyrins with the anionic axial ligands is slightly delocalized toward the chlorine and sulfur, while the spin density at the $N_\epsilon$ atom of imidazole is negative due to polarization effects.

**B. Electronic Ground State of Compound I.** The compound I intermediate is derived from compound II by one-electron oxidation. It has been shown in the previous section that the HOMO's of compound II comprise three kinds of orbitals: MO's with mainly iron 3d character, the porphyrin $a_{1u}$- and $a_{2u}$-type MO's, and MO's with predominant contribution from the axial ligand. Since these MO's are in the same energy range, several possibilities for oxidation of compound II are conceivable. If the electron is removed from one of the orbitals with mainly iron 3d character, the resulting complex is formally an oxoiron(V) porphyrin. Up to now, conclusive experimental evidence does not exist on oxoiron(V) porphyrin, and a calculation shows that the cationic state obtained by ionization of the $3d_{xy,\beta}$ orbital lies 1.34 eV above the ground state for the $Cl^-$-coordinated species. Oxidation of the porphyrin core results in an oxoiron(IV) porphyrin radical complex with either $A_{1u}$ or $A_{2u}$ character.[53] Most of the experimental results support this assignment, and both types of porphyrin radicals have been detected.[5−13,15,16,18−22,24−29] In the third case the radical resides on the axial ligand, a possibility that has been considered only recently.[54] Furthermore, ionization of either an $\alpha$ spin or a $\beta$ spin orbital is possible. Finally, it should be mentioned that in some native systems the radical has been detected on a distal amino acid.[55,56] This case apparently can not be dealt with in this work.

**TABLE 5: Average Binding Energy $\bar{E} = (E(3/2) + E(1/2))/2$ Relative to the $A^\bullet_{2u}$ State for Compound I Analogues with the Radical Located in Different MO's and Exchange Coupling Constant $J$ of the Heisenberg Hamiltonian $H = -J\vec{S}\cdot\vec{S}'$ [a]**

| state | | O═FeP | $Cl^-$ | Imi | $H3CS^-$ |
|---|---|---|---|---|---|
| $A^\bullet_{2u}$ | $\bar{E}$ [eV] | 0.0 | 0.0 | 0.0 | 0.0 |
| | $J$ [$cm^{-1}$] | −210 | +69 | +51 | +186 |
| $A^\bullet_{1u}$ | $\bar{E}$ [eV] | 0.409 | 0.438 | 0.421 | 0.744 |
| | $J$ [$cm^{-1}$] | −27 | −18 | −30 | +77 |
| $L.P.^\bullet_\perp$ | $\bar{E}$ [eV] | | 0.933 | 3.094 | −0.922 |

[a] Values for the $L.P.^\bullet_\perp$ state are not given, since mixing between the magnetic orbitals yields unreasonable results.

Table 5 displays the energies of the low-lying states of compound I with different axial ligands. The ground state for the chlorine- and imidazole-ligated systems is obtained by ionization of the $a_{2u,\beta}$ orbital, while for the five-coordinated species ionization of the $a_{2u,\alpha}$ orbital yields the state with the lowest energy. In all three cases formation of the $A^\bullet_{1u}$ state requires about 0.4 eV more energy. The magnitude of the splitting between states derived from ionization of corresponding $\alpha$ and $\beta$ orbitals is about 1% of the $A^\bullet_{1u}/A^\bullet_{2u}$ spacing. In case of chlorine-ligated porphyrin the axial ligand lone-pair radical lies about 1 eV above the ground state. This is in accordance with the result that the l.p. MO in the ground state of compound II lies approximately 1 eV below the $a_{2u}$. However, with $H_3CS^-$ as axial ligand, the $l.p._\perp$ MO is the HOMO of compound II, and the corresponding cationic state, $L.P.^\bullet_\perp$,[57] constitutes the ground state of compound I. The $A^\bullet_{2u}$ state lies about 1 eV higher and is, in addition, stabilized with respect to the $A^\bullet_{1u}$ state by 0.7 eV. This is also reflected in the MO energy diagram of compound II (Figure 5). States that are created by oxidation of an electron out of the $3d_{xy}$ orbital are more than 1 eV above the ground state, but ionization of the $(pd\pi)^*$ orbital leads to a low-lying state between the $A^\bullet_{1u}$ and $A^\bullet_{2u}$ states for the chlorine-coordinated system.

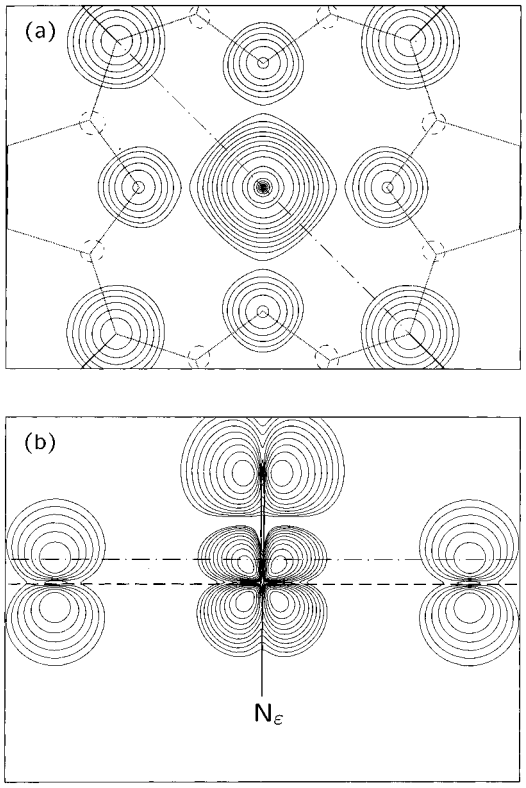


**Figure 6.** Spin density in the ground state of compound I with imidazole as axial ligand: (a) plot of plane parallel to the porphyrin plane; (b) plot of plane perpendicular to the porphyrin and the axial ligand plane. The dash-dotted line in (a) indicates the plot plane of (b) and vice versa. The dashed line in (b) is the porphyrin plane. Contour lines are at −0.0015, 0.0015, 0.0025, 0.0042, 0.0070, 0.0116, 0.0194, 0.0323, 0.0539, 0.0898, and 0.1499 multiplied $\hbar/2a_0^3$.

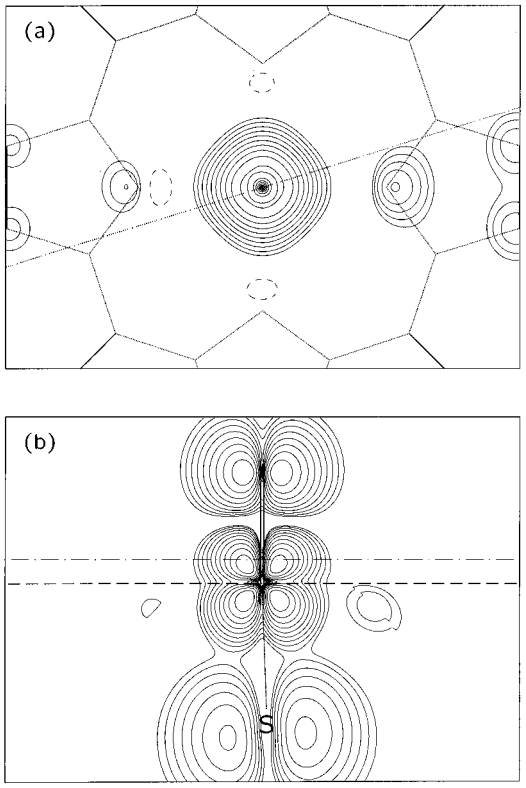


**Figure 7.** Spin density in the ground state of compound I with $H_3CS^-$ as axial ligand.

**TABLE 6: Effective Atomic Charges *Q* (in e), Spin Density *σ* (in ħ/2) and Overlap Population (in e) for Low-Lying States of the Compound I Analogue with $H_3CS^-$ as Axial Ligand[b]**

| atom | | L.P.$^\bullet_\perp$(3/2) | L.P.$^\bullet_\perp$(1/2) | $A^\bullet_{1u}$ (3/2) | $A^\bullet_{2u}$ (1/2) | $A^\bullet_{1u}$ (3/2) | $A^\bullet_{1u}$ (1/2) |
|---|---|---|---|---|---|---|---|
| N | *Q* | −0.20 | −0.20 | −0.18 | −0.18 | −0.19 | −0.19 |
| | *σ* | 0.012[a] | −0.022 | 0.081 | −0.129 | −0.046 | −0.005 |
| $C_\alpha$ | *Q* | 0.03 | 0.04 | 0.04 | 0.04 | 0.06 | 0.06 |
| | *σ* | 0.013 | −0.026 | −0.018 | 0.021 | 0.120 | −0.117 |
| $C_\beta$ | *Q* | 0.01 | 0.01 | 0.01 | 0.01 | 0.02 | 0.02 |
| | *σ* | 0.015 | −0.010 | −0.001 | −0.001 | 0.025 | −0.027 |
| $C_m$ | *Q* | 0.04 | 0.04 | 0.07 | 0.07 | 0.05 | 0.05 |
| | *σ* | −0.001 | 0.003 | 0.139 | 0.138 | −0.020 | 0.021 |
| S | *Q* | −0.14 | −0.22 | −0.34 | −0.35 | −0.40 | −0.40 |
| | *σ* | 0.697 | −0.508 | 0.219 | −0.091 | 0.036 | 0.032 |
| O | *Q* | −0.51 | −0.49 | −0.55 | −0.54 | −0.57 | −0.57 |
| | *σ* | 0.922 | 0.818 | 0.887 | 0.811 | 0.852 | 0.854 |
| Fe | *Q* | 0.94 | 0.98 | 0.91 | 0.92 | 0.88 | 0.88 |
| | *σ* | 1.176 | 1.057 | 1.183 | 1.165 | 1.213 | 1.195 |

| bond | L.P.$^\bullet_\perp$(3/2) | L.P.$^\bullet_\perp$(1/2) | $A^\bullet_{1u}$ (3/2) | $A^\bullet_{2u}$ (1/2) | $A^\bullet_{1u}$ (3/2) | $A^\bullet_{1u}$ (1/2) |
|---|---|---|---|---|---|---|
| Fe−N | 0.195 | 0.193 | 0.188 | 0.187 | 0.187 | 0.187 |
| Fe−S | 0.135 | 0.179 | 0.161 | 0.165 | 0.179 | 0.179 |
| Fe═O | 0.535 | 0.538 | 0.538 | 0.540 | 0.546 | 0.546 |

[a] See footnote b of Table 4. [b] Average values are given for the atoms of the porphyrin macrocycle and for Fe−N.

The charge distributions of all compound I species closely resemble the charge distributions of the corresponding compound II species (Table 4). For the systems with the radical on the porphyrin macrocycle, i.e., the five- and six-coordinated compound I species with chlorine and with imidazole as axial ligands, the effective atomic charges of the pyrroline nitrogen and methine carbon atoms increase by 0.05 in going from compound II to compound I, while an increase of 0.03 for the $C_\alpha$ and 0.01 for the $C_\beta$ atoms is obtained. The larger increase in charge of the pyrroline nitrogen and the methine carbon atoms compared with the pyrroline carbon atoms ($C_\alpha$, $C_\beta$) is in accordance with the $a_{2u}$ character of the radical orbital. However, it is less than the expected value of about 1/8 because the radical orbital is shielded by the remaining electrons because of orbital relaxation of the occupied valence orbitals so that some charge is removed from the oxygen and the coordinating atom of the axial ligand.

For compound I with $H_3CS^-$ as axial ligand, the radical orbital is located at the sulfur atom. Hence, the change in the effective charges of the porphyrin atoms is smaller upon oxidation of $H_3CS^-$ ligated compound II, while that of the axial ligand (by 0.27) and of oxygen (by 0.08) is larger (cf. Table 4) than in the other cases. In all cases the effective charge of the iron decreases slightly. This is caused by an increase in the occupation of the Fe(4s) and Fe(4p) AO's that overcompensates the decrease of the Fe(3d) population. The overlap population of the Fe═O bond is 5% and of the Fe−N bond 10% larger in compound I than in compound II (Table 4).

The spin density distribution of compound I (Table 4) expresses the radical character better than does the charge distribution. Compared with the corresponding compound II systems, the spin density in compound I with a porphyrin-centered radical becomes positive on the nitrogens and the methine carbon atoms for the six-coordinated and negative for the five-coordinated species because a $\beta$ spin orbital is ionized in the former and an $\alpha$ spin orbital in the latter case. The change in spin density on the nitrogen is −0.068 for the five-coordinated system, 0.126 and 0.112 for the chlorine- and imidazole-ligated six-coordinated systems, and −0.165, 0.176, and 0.180 on the methine carbon atom, respectively, in good agreement with the expected average value of 1/8. The change in spin density of the pyrroline carbon atoms is smaller. The spin density at the coordinating atom of the axial ligand is slightly increased to 0.039 for Cl and to 0.016 for $N_\epsilon$ of imidazole, while the spin

density at the oxygen atom remains almost constant upon oxidation. Figure 6 displays the spin density distribution of the imidazole-coordinated compound I analogue.

With $H_3CS^-$ as the axial ligand, the total change of the spin density on the porphyrin is small, except for an increase by 0.106 at the nitrogen atom in $+x$ direction. The dominant part of the spin density in compound I is found at the sulfur atom with 0.697 (Figure 7), accompanied by a slight increase of the oxygen spin density of 0.056 (Table 4). The spin density of iron is slightly lowered in all cases, namely by $-0.025$ for chlorine, $-0.035$ for imidazole, $-0.037$ for $H_3CS^-$, and $-0.129$ for the five-coordinated case. Altogether, the charge and spin density distribution within the Fe═O subunit is rather similar for all four systems, regardless of the nature of the axial ligand, the site of oxidation, and the different excited hole states of compound I as shown, representatively, for the $H_3CS^-$ ligated system in Table 6. This result confirms that the charge and spin density within the Fe═O subunit is not an essential indicator for the reactivity of compound I systems.[49]

**C. Exchange Coupling.** The coupling of the spin $\mathfrak{S}$ of the oxoiron(IV) subunit with the radical spin $\mathfrak{S}'$ generated by oxidation of compound II is described within the frame of the spin Hamiltonian formalism[58] by the Heisenberg Hamiltonian $H = -J\mathfrak{S}\cdot\mathfrak{S}'$. The isotropic coupling constant $J$ can be derived within the broken spin symmetry formalism[59] from the expression

$$J = -2\,\frac{E(S_{max}) - E(S_{min})}{S_{max}^{\,2} - S_{min}^{\,2}} \qquad (1)$$

with $E(S)$ being the binding energy of the system in the spin state $S$. Taking into account that in the present case the total spin can take maximum and minimum values of $S_{max} = 3/2$ and $S_{min} = 1/2$, the coupling constant $J$ is equal to the energy difference between the states with parallel and antiparallel coupling of the two spins. The corresponding energy difference is on the order of 0.01% of the binding energies calculated for the two states separetely. The coupling constants for the $A^{\bullet}_{2u}$ state are calculated as $J = +69$ cm$^{-1}$ and $J = +51$ cm$^{-1}$ for the chlorine- and imidazole-ligated compound I analogues, respectively (Table 5). In case of the five-coordinated compound I analogue the coupling is stronger and antiparallel, $J$ $-210$ cm$^{-1}$. For the $A^{\bullet}_{1u}$ state $J$ varies between $-18$ and $-30$ cm$^{-1}$, i.e., the porphyrin radical spin exhibits weak antiferromagnetic coupling to the spin of the Fe═O subunit for all three cases. For the $H_3CS^-$ ligated system both the $A^{\bullet}_{2u}$ and the $A^{\bullet}_{1u}$ spin state is $S = 3/2$ with values for the coupling constants of $J = +186$ and $J = +77$ cm$^{-1}$, respectively.

Because the coupling constants represent small energies on the scale of the binding energies, the results may be sensitive to the geometrical assumptions underlying the calculation. However, even the reference model system with chlorine as the axial ligand contains 39 atoms, resulting in 111 degrees of freedom for changing the geometry so that the investigation of the dependence of $J$ on all these conceivable variations is impossible. To restrict the number of geometrical parameters, the porphyrin core and the axial ligand are considered as rigid, and only the influence of the relative orientation of the axial ligand on $J$ will be investigated.

For the compound I analogue with a chlorine anion as the axial ligand, the dependence of $J$ on the Fe—Cl, Fe═O, and Fe—N[60] bond distances are examined (Table 7). Increasing the iron—chlorine distance from 2.2 to 2.3 Å influences the coupling strength only slightly with a change of $J$ from $+69$ cm$^{-1}$ to $+82$ cm$^{-1}$, while elongating the iron—oxygen distance to 1.75 Å results in $J = +141$ cm$^{-1}$. For the porphyrin with the smaller iron—nitrogen distance of 1.97 Å, the coupling constants $J = +76$ and $+95$ cm$^{-1}$ closely resemble the values for d(Fe—N) = 2.04 Å. The decrease in total energy by $-0.03$ eV indicates that the iron—nitrogen distance in highly oxidized oxoiron(IV) porphyrins may actually be smaller than the value of 2.04 Å chosen in this work. Enlarging the Fe—$N_\epsilon$ distance by 0.1 Å in the imidazole-ligated compound I analogue yields a similar increase of the coupling strength from $J = +51$ to $+60$ cm$^{-1}$ (Table 8) as obtained for the analogous geometrical variation in the chlorine-ligated system. The values for $J$ are virtually independent of the rotation angle $\beta$ around the $z$ axis, but tilting the axial ligand by $\alpha_{||}$ (Figure 3) within the imidazole plane in such a way that the $H_\epsilon$ atom (cf. Figure 2) moves toward the porphyrin plane leads to significant changes of the coupling strength in the $A^{\bullet}_{2u}$ state. Passing from $\alpha_{||} = 0°$ to 5° reduces the value of the coupling constant from $+51$ to $-4$ cm$^{-1}$. An increase of the tilting angle $\alpha_{||}$ to 10° and 20° results in values of $J = -118$ and $-475$ cm$^{-1}$, i.e., the coupling becomes strongly antiferromagnetic. At the same time, however, the total energies relative to the case for $\alpha_{||} = 0°$ increase by 0.11 eV for 5°, by 0.67 eV for 10°, and by 2.0 eV for 20°. These results indicate that the porphyrin core will not stay planar under such a change in geometry. A similar influence of the axial ligand on the distortion of the porphyrin core has recently been demonstrated for a series of iron(II) porphyrinates.[61] The coupling constant of the $A^{\bullet}_{1u}$ state and the $A^{\bullet}_{1u}/A^{\bullet}_{2u}$ splitting are practically unaffected by these geometrical variations within the compound I analogue with chlorine and imidazole as axial ligands.

When the iron of the five-coordinated compound I analogue is moved out of the porphyrin plane by 0.5 Å into the direction of the oxygen atom while keeping the oxoiron distance constant, the $A^{\bullet}_{2u}$ coupling constant changes monotonically from $J =$

**TABLE 7: Exchange Coupling Constant $J$ (in cm$^{-1}$) of the Heisenberg Hamiltonian $H = -J\vec{S}\cdot\vec{S}'$ for Chlorine-Coordinated Compound I Analogues with the Radical Located in Porphyrin $\pi$ MO's**

| | | | | | | |
|---|---|---|---|---|---|---|
| | Fe—N | 2.04 Å | 2.04 Å | 2.04 Å | 1.97 Å | 1.97 Å |
| | Fe—Cl | 2.2 Å | 2.3 Å | 2.2 Å | 2.3 Å | 2.2 Å |
| | Fe—O | 1.65 Å | 1.65 Å | 1.75 Å | 1.65 Å | 1.65 Å |
| state | $A^{\bullet}_{2u}$ | +69 | +82 | +141 | +95 | +76 |
| | $A^{\bullet}_{1u}$ | −18 | −20 | −23 | −23 | −21 |

**TABLE 8: Exchange Coupling Constant $J$ (in cm$^{-1}$) of the Heisenberg Hamiltonian $H = -J\vec{S}\cdot\vec{S}'$ for Imidazole-Coordinated Compound I Analogues with the Radical Located in Porphyrin $\pi$ MO's**

| | | | | | | | |
|---|---|---|---|---|---|---|---|
| | Fe—$N_\epsilon$ | 2.1 Å | 2.1 Å | 2.1 Å | 2.1 Å | 2.2 Å | |
| | $\alpha$ | 0° | 0° | 0° | 0° | 0° | |
| | $\beta$ | 0° | 15° | 30° | 45° | 45° | |
| state | $A^{\bullet}_{2u}$ | +54 | +54 | +52 | +51 | +60 | |
| | $A^{\bullet}_{1u}$ | −28 | −31 | −29 | −30 | −27 | |
| | Fe—$N_\epsilon$ | 2.1 Å | 2.1 Å | 2.1 Å | 2.1 Å | 2.2 Å | 2.1 Å |
| | $\alpha_{||}$ | 5° | 5° | 5° | 10° | 10° | 10° |
| | $\alpha_\perp$ | 0° | 0° | 0° | 0° | 0° | 0° |
| | $\beta$ | 0° | 21.2° | 45° | 0° | 21.2° | 45° |
| state | $A^{\bullet}_{2u}$ | +1 | −1 | −4 | −94 | −105 | −118 |
| | $A^{\bullet}_{1u}$ | −28 | −27 | −28 | −34 | −28 | −28 |
| | Fe—$N_\epsilon$ | | 2.1 Å | | 2.1 Å | | 2.1 Å |
| | $\alpha_{||}$ | | 20° | | 20° | | 20° |
| | $\alpha_\perp$ | | 0° | | 0° | | 0° |
| | $\beta$ | | 0° | | 21.2° | | 45° |
| state | $A^{\bullet}_{2u}$ | | −385 | | −420 | | −475 |
| | $A^{\bullet}_{1u}$ | | −168 | | −37 | | −28 |

**TABLE 9: Exchange Coupling Constant $J$ (in cm$^{-1}$) of the Heisenberg Hamiltonian $H = -JS\cdot S'$ for Five-Coordinated Compound I Analogues with the Radical Located in Porphyrin $\pi$ MO's**

| | Fe−N | 2.04 Å | 2.05 Å | 2.05 Å | 2.06 Å | 2.08 Å | 2.10 Å |
|---|---|---|---|---|---|---|---|
| | Fe−Ct | 0.0 Å | 0.1 Å | 0.2 Å | 0.3 Å | 0.4 Å | 0.5 Å |
| state | $A_{2u}^{\bullet}$ | −210 | −176 | −123 | −58 | +26 | +117 |
| | $A_{1u}^{\bullet}$ | −27 | −19 | −12 | −7 | −3 | +1 |

**TABLE 10: Exchange Coupling Constant $J$ (in cm$^{-1}$) of the Heisenberg Hamiltonian $H = -JS\cdot S'$ for $H_3CS^-$-Coordinated Compound I Analogues with the Radical Located in Porphyrin $\pi$ MO's**

| | Fe−S | 2.16 Å | 2.21 Å | 2.26 Å | 2.31 Å | 2.26 Å | 2.2 Å |
|---|---|---|---|---|---|---|---|
| | $\alpha_{\|\|}$ | 6.0° | 5.9° | 5.8° | 5.6° | 0.0° | 0.0° |
| | $\alpha_{\perp}$ | 2.3° | 2.2° | 2.2° | 2.1° | 0.0° | 0.0° |
| | $\beta$ | 107.3° | 107.3° | 107.3° | 107.3° | 0.0° | 21.2° |
| state | $A_{2u}^{\bullet}$ | −708 | −205 | +242 | +186 | −2037 | −1307 |
| | $A_{1u}^{\bullet}$ | +43 | +43 | +51 | +77 | +376 | +231 |

−210 to +117 cm$^{-1}$ (Table 9) and the total energy increases by 1.1 eV. The binding energy takes a minimum for a 0.1 Å out-of-plane displacement of the iron with −0.1 eV below the in-plane position and $J = -176$ cm$^{-1}$. The same geometrical change causes a change of the $A_{1u}^{\bullet}$ coupling constant from −27 cm$^{-1}$ to approximately zero.

In the $H_3CS^-$ ligated compound I analogue, the coupling constants are much more sensitive to geometrical variation than in the other three cases (Table 10). Especially remarkable is the sensitivity to changing the angle $\alpha$ from 6° to 0°. The values of $J$ calculated for the $A_{2u}^{\bullet}$ state vary between −2037 and +186 cm$^{-1}$ for changes of the iron−sulfur distance between 2.15 and 2.31 Å and of the rotation angle $\beta$ between 0° and 21.2°.[62] For the $A_{1u}^{\bullet}$ state the coupling is always ferromagnetic and $J$ ranges from +43 to +376 cm$^{-1}$. For all considered geometries the ground state corresponds to the lone-pair sulfur radical state L.P.$^{\bullet}$, while the $A_{2u}^{\bullet}$ state is always located about 1 eV above. However, the magnetic ligand orbital has more than 10% contribution from the Fe═O centered magnetic orbital (Table 3) so that the applicability of the Heisenberg model may be questioned for a quantitative determination of $J$ for the L.P.$^{\bullet}$ state. Accordingly, calculated $J$ values vary between +1478 and −360 cm$^{-1}$ for the examined geometries, and further geometrical modifications may even enlarge this range. The spin state of this ground state is obtained as the doublet ($S = 1/2$) for Fe−S distances below about 2.2 Å, while for larger distances the quartet ($S = 3/2$) is lower in energy.

## IV. Discussion

The results of our calculations will now be compared with theoretical results obtained by other methods of similar sophistication, viz. CASSCF[34,35] and the fully numerical LDA,[40] and with experimental data. The spin density distribution within the Fe═O unit obtained with all three theoretical methods compares well with each other. CASSCF yields a spin density of 1.12 at the iron and of 0.86 at the oxygen for a pyridine-coordinated compound II analogue,[34] which is very close to our values of 1.187 and 0.914 for the imidazole-ligated system (Table 4). The numerical LDA calculation for a five-coordinated compound II model yields a spin density on the Fe and O atoms of 1.196 and 0.821, respectively,[40] in good agreement with our values of 1.253 and 0.934 given in Table 4 for the five-coordinated system. The effective atomic charge of 2.37 for iron obtained in CASSCF[34] is considerably larger than our result of 0.98 for the imidazole-ligated system, whereas the charge of 0.50 for iron in the LDA calculation[40] is smaller than our value of 0.93 for the five-coordinated compound II analogue (Table 4). The charges of the oxygen obtained by CASSCF (−0.49) and by LDA (−0.40) are both in good agreement with the corresponding SCC-X$\alpha$ values of −0.51 and −0.47, respectively (Table 4).

In all calculations the charge and spin density distributions within the Fe═O unit remain essentially the same in going from compound II to compound I. For the $A_{2u}^{\bullet}$ state the CASSCF calculation gives spin densities of 1.10 for Fe and 0.89 for O,[35] and the corresponding LDA values are 1.184 (Fe) and 0.849 (O).[40] The respective values of our calculation are 1.152 and 0.920 for the imidazole-coordinated and 1.124 and 0.933 for the five-coordinated compound I analogue in Table 4. Common to all calculations is thus a slight transfer of spin density from the iron to the oxygen upon oxidation. The variation of the effective charges is even smaller: the values of 2.25 and −0.43 on iron and oxygen, respectively, calculated by CASSCF[35] and the values of 0.52 and −0.36 of the LDA calculation[40] are almost identical with the compound II results, as in the SCC-X$\alpha$ calculation of this work (Table 4). Altogether, these results show that the electronic structure of the Fe═O bond is essentially insensitive to the removal of an electron from a porphyrine $\pi$ orbital, as mentioned earlier.[35] On the basis of our calculations, we can further conclude that the charge and spin density distributions within the Fe═O subunit are virtually independent of the nature of the axial ligand. Analogous results have been obtained by semiemperical INDO calculations.[33] In addition, the properties of the Fe═O moiety are largely unaffected even when removing an electron from the l.p. orbital of the axial ligand (Table 6).

Exchange coupling constants of porphyrin cation radical complexes have not yet been computed to our knowledge by other electronic structure methods so that they can be compared only with experimentally derived values. Such a comparison, however, is restricted in several respects from both the theoretical and the experimental side. As to the theoretical side, all calculations are based on the geometrical model assumption of a planar symmetric porphyrin core without any terminal substituents. The effects of terminal substituents and distortions of the porphyrin core on the electronic structure of compound I and compound II analogues have been studied in a separate investigation.[41] This analysis yields, among other results, the conclusion that slight distortions of the porphyrin core with deviations up to 0.05 Å from the root mean square plane lead to variations in $J$ below 50% and do not change the sign. Therefore, agreement with experimental values can be expected at best within these limits.

Regarding the experimental side, the Mössbauer and EPR spectra of compound I species are often superimposed by signals from the reduced species (compound II) and/or ferric precursors because it is practically impossible to synthesize compound I analogues with 100% yield. This precludes the determination of $J$ from temperature-dependent magnetic susceptibility measurements so that $J$ has to be derived from spin Hamiltonian simulations of Mössbauer and EPR spectra only. Since in this case $J$ is strongly covariant with the zero-field splitting parameter $D$ and the local $g$ values of iron(IV), the simulation usually leads to a manifold of solutions with $J$ given at best with an accuracy of ±20%.[63,64] This has to be kept in mind when comparing calculated and measured exchange coupling constants.

Experimentally derived $J$ values for synthetic models of compound I of oxoiron(IV) tetramesitylporphyrin[63] cover the range +42.6 to +57.0 cm$^{-1}$, in close agreement with the computed value of +69 cm$^{-1}$ for the $A_{2u}^{\bullet}$ cationic state (Table

5). An EPR investigation of three compound I analogues with methanol as the second axial ligand yields $J = +43$ cm$^{-1}$ for tetramesitylporphyrin, $J = +38$ cm$^{-1}$ for tetrakis(2,6-dichlorophenyl)porphyrin, and $J = +22$ cm$^{-1}$ for tetrakis(2,4,6-trimethoxyphenyl)porphyrin.[11] The corresponding SCC-X$\alpha$ value for the $A^{\bullet}_{2u}$ state of a compound I analogue with methanol[65] as the axial ligand and without peripheral ring substituents amounts to $+34$ cm$^{-1}$. Finally, recent experimental studies[13,66] on model systems with the $A^{\bullet}_{1u}$ ground state yield ferromagnetic coupling constants of about $+10$ cm$^{-1}$, being significantly smaller compared to values from $A^{\bullet}_{2u}$ type systems. The calculated coupling constants for $A^{\bullet}_{1u}$ states show a similar decrease in strength.

In Table 11 experimental values of the exchange coupling constant $J$ obtained for biomimetic model complexes are compared with those of native peroxidases. The $J$ values of all model complexes cover the range from moderate to strong ferromagnetic coupling. However, none of them reproduces very weak coupling as observed in horseradish peroxidase or antiferromagnetic coupling as in chloroperoxidase.[54] It is therefore interesting to note under which conditions our calculations yield small or negative $J$ values. For the imidazole-coordinated compound I reference system the calculated value amounts to $J = +51$ cm$^{-1}$ (Table 5). Tilting of the axial imidazole ligand changes this result to negative values (Table 8), and a tilting angle $\alpha_{||}$ of 5° can reproduce the observed weak coupling $-2.6$ ... $+2.6$ cm$^{-1}$ in horseradish peroxidase.[6] The energy needed for such minor geometrical variations can easily be supplied by the protein environment. In the $H_3CS^-$ coordinated compound I model system, the quantitative determination of $J$ is precluded by the limited applicability of the Heisenberg model because of mixing between the magnetic orbitals as mentioned above.

In summary, the coupling between the oxoiron(IV) and the radical spin in compound I depends in a complicated way on the coordination environment of the heme iron. Therefore, conclusions drawn from a single $J$ value with respect to structural properties of the heme group cannot be expected to be unequivocal because different types of coordinations and geometries may lead to the same spin coupling. Implications of the coupling mode and strength on catalytic properties seem unlikely because the $J$ values represent small energies on the scale of reaction enthalpies and potential barriers. Furthermore, the electronic structure of the heme group alone does not serve as an indicator of its reactivity, but instead, the orbital interactions between the heme group and the substrate along the whole reaction pathway have to be considered.[49]

## V. Summary

The results presented in this investigation demonstrate that molecular orbital calculations within the local density approximation yield qualitatively reliable results for electronic properties of compound I and compound II as a function of the axial ligand. The ground state configuration found for compound II is the ferryl $(t_{2g})^4$ configuration $(3d_{xy})^2(3d_{xz},3d_{yz})^2$ with total spin $S = 1$ in all cases. Two unpaired electrons occupy the antibonding $(pd\pi)^*$ MO's consisting of iron $3d_{xz}$, $3d_{yz}$ and oxygen $2p_x$, $2p_y$ atomic orbitals (AO's) and give rise to a spin density that is almost completely localized within the oxoiron(IV) unit with a distribution of approximately 60/40 between the iron and oxygen atom. The main influence of the axial ligand on the electronic properties is 2-fold: (i) the $a_{2u}$ MO and the $t_{2g}$ MO's $3d_{xy}$ and $(pd\pi)^*$ are destabilized relative to the $a_{1u}$ MO; (ii) an additional orbital with ligand lone-pair (l.p.) character lies 1 and 4 eV below the HOMO $a_{2u}$ in the chlorine- and imidazole-ligated complexes, respectively, but above $a_{2u}$ for $H_3CS^-$ and becomes itself the HOMO. Correspondingly, the ground state of compound I is the $A^{\bullet}_{2u}$ state in the former two cases, as well as in the five-coordinated oxoiron(IV) porphyrin radical, whereas it changes to the L.P.$^{\bullet}$ state in the $H_3CS^-$ coordinated case. The additional spin density of compound I induced by the oxidation of compound II is distributed mainly over the pyrroline nitrogen and methine carbon atoms for the porphyrin-centered magnetic orbital $a_{2u}$ (Figure 6) and is mainly localized on the sulfur atom for the ligand-centered one (Figure 7). The electronic structure of the Fe=O bond is remarkably unaffected by the nature of the axial ligand, as well as by the type of the radical orbital.

**TABLE 11: Experimental Values for the Exchange Coupling Constant $J$ (in cm$^{-1}$)[j]**

| system | axial ligand | $D$ [cm$^{-1}$] | $J$ [cm$^{-1}$] | ref |
|---|---|---|---|---|
| TMP[a]−I | chlorine | +25 | +42.6 ... +57.0 | 63 |
| TMP[a]−I | methanol[i] | +25 | +43 | 11 |
| TDCPP[b]−I | methanol[i] | +25 | +38 | 11 |
| TTMPP[c]−I | methanol[i] | +20 | +22 | 11 |
| TMTMP[d]−I | methanol | +28 | +8 | 63 |
| TMTMP[d]−I | methanol | +20 | +12 | 66 |
| HRP[e]−I | imidazole | +26 | −2.6 ... +2.6 | 6 |
| CPO[f]−I | thiolate | +36 | −36.8 | 7 |
| CAT[g]−I | phenolate | $D > 0$ | 0.4$D$ | 29 |
| APX[h]−I | imidazole | $D > 0$ | 0.28$D$ | 67 |

[a] Tetramesitylporphyrin. [b] Tetra(2,6-dichlorophenyl)porphyrin. [c] Tetra(2,4,6-trimethoxyphenyl)porphyrin. [d] Tetramethyltetramesitylporphyrin. [e] Horseradish peroxidase. [f] Chloroperoxidase. [g] Catalase. [h] Ascorbate peroxidase. [i] D. Mandon, personal communication. [j] The literature values are converted to fit the convention of the Heisenberg Hamiltonian $H = -J\mathbf{S}\cdot\mathbf{S}'$ used in this work, if necessary.

Calculation of the isotropic part of the exchange coupling constant $J$ for the spin coupling between the oxoiron and the radical spin in six-coordinated compound I yields parallel alignment between both spins in the $A^{\bullet}_{2u}$ state, while for the five-coordinated oxoiron(IV) porphyrin radical with in-plane iron antiparallel spin-orientation is favored energetically. In the $A^{\bullet}_{1u}$ state the spin coupling is estimated to be distinctly weaker and antiferromagnetic in all cases except for the $H_3CS^-$ ligated system (Table 5). Mode and strength of spin coupling are sensitive against geometrical variations. Although changing the iron−ligand bond distance and rotating the ligand around the direction perpendicular to the porphyrin plane in imidazole-ligated compound I do not alter the mode of spin coupling in the $A^{\bullet}_{2u}$ state, tilting the axial ligand toward the porphyrin plane produces strong antiferromagnetic coupling. The spin coupling in the $A^{\bullet}_{1u}$ state is almost independent of the orientation of imidazole (Table 8). Geometrical variation of the axial ligand $H_3CS^-$ does not change the separation between the L.P.$^{\bullet}$ ground state and the $A^{\bullet}_{2u}$ excited state of ca. 1 eV but strongly influences the sequence of the quartet and doublet L.P.$^{\bullet}$ states. For iron−sulfur distances larger than about 2.2 Å, the ground state is the quartet state, while for smaller distances the doublet state is lower in energy.

**Acknowledgment.** This work was supported by the German Research Foundation (DFG) and the EU Human Capital and Mobility Grant MASIMO (ERB CHRX-CT92-0072). We gratefully acknowledge the stimulating discussions with O. Zakharieva, D. Mandon, R. Weiss, I. M. C. M. Rietjens, and C. Veeger.

## References and Notes

(1) Everse, J., Everse K. E., Grisham M. B., Eds. *Peroxidases in Chemistry and Biology*; CRC Press: Boca Raton, Ann Arbor, Boston, 1991; Vols. I and II.

(2) Ortiz de Montellano, P. R., Ed. *Cytochrome P-450. Structure, Mechanism, and Biochemistry*; Plenum Press: New York and London, 1986.
(3) Schappacher, M.; Weiss, R.; Montiel-Montoya, R.; Trautwein, A. X.; Tabard, A. *J. Am. Chem. Soc.* **1985**, *107*, 3736.
(4) Andersson, L. A.; Dawson, J. H. *Struct. Bonding* **1990**, *74*, 1.
(5) Schulz, C. E.; Devaney, P. W.; Winkler, H.; Debrunner, P. G.; Doan, N.; Chiang,R.; Rutter, R.; Hager, L. P. *FEBS Lett.* **1979**, *103*, 102.
(6) Schulz, C. E.; Rutter, R.; Sage, J. T.; Debrunner, P. G.; Hager, L. P. *Biochemistry* **1984**, *23*, 4743.
(7) Rutter, R.; Hager, L. P.; Dhonau, H.; Hendrich, M.; Valentine, M.; Debrunner, P. G. *Biochemistry* **1984**, *23*, 6809.
(8) Boso, B.; Lang, G.; McMurray, T. J.; Groves, J. T. *J. Chem. Phys.* **1983**, *79*, 1122.
(9) Gold, A.; Jayaraj, K.; Doppelt, P.; Weiss, R.; Chottard, G.; Bill, E.; Ding, X.-Q.; Trautwein, A. X. *J. Am. Chem. Soc.* **1988**, *110*, 5756.
(10) Bill, E.; Ding, X.-Q.; Bominaar, E. L.; Trautwein, A. X.; Winkler, H.; Mandon, D.; Weiss, R.; Gold, A.; Jayaraj, K.; Hatfield, W. E.; Kirk, M. L. *Eur. J. Biochem.* **1990**, *188*, 665.
(11) Mandon, D.; Weiss, R.; Jayaraj, K.; Gold, A.; Terner, J.; Bill, E.; Trautwein, A. X. *Inorg. Chem.* **1992**, *31*, 4404.
(12) Jayaraj, K.; Gold, A.; Austin, R. N.; Mandon, D.; Weiss, R.; Terner, J.; Bill, E.; Müther, M.; Trautwein, A. X. *J. Am. Chem. Soc.* **1995** *117*, 9079.
(13) Fujii, H.; Yoshimura, T.; Kamada, H. *Inorg. Chem.* **1996**, *35*, 2373.
(14) Chin, D.-H.; Balch, A. L.; LaMar, G. N. *J. Am. Chem. Soc.* **1980**, *102*, 1446.
(15) Groves, J. T.; Haushalter, R. C.; Nakamura, M.; Nemo, T. E.; Evans, B. J. *J. Am. Chem. Soc.* **1981**, *103*, 2884.
(16) Balch, A. L.; Latos-Grazynski, L.; Renner, M. W. *J. Am. Chem. Soc.* **1985**, *107*, 2983.
(17) Balch, A. L.; LaMar, G. N.; Latos-Grazynski, L.; Renner, M. W.; Thanabal, V. *J. Am. Chem. Soc.* **1985**, *107*, 3003.
(18) Gross, Z.; Nimri, S. *Inorg. Chem.* **1994**, *33*, 1731.
(19) Gross, Z.; Nimri, S. *J. Am. Chem. Soc.* **1995**, *117*, 8021.
(20) Groves, J. T.; Watanabe, Y. *J. Am. Chem. Soc.* **1986**, *108*, 507.
(21) Groves, J. T.; Watanabe, Y. *J. Am. Chem. Soc.* **1988**, *110*, 8443.
(22) Fujii, H. *J. Am. Chem. Soc.* **1993**, *115*, 4641.
(23) Mizutani, Y.; Hashimoto, S.; Tatsuno, Y.; Kitagawa, T. *J. Am. Chem. Soc.* **1990**, *112*, 6809.
(24) Hashimoto, S.; Mizutani, Y.; Tatsuno, Y.; Kitagawa, T. *J. Am. Chem. Soc.* **1991**, *113*, 6542.
(25) Proniewicz, L. M.; Paeng, I. R.; Nakamoto, I. K. *J. Am. Chem. Soc.* **1991**, *113*, 3294.
(26) Ogura, T.; Takahashi, S.; Hirota, S.; Shinzawa-Itoh, K.; Yoshikawa, S.; Appelman, E. H.; Kitagawa, T. *J. Am. Chem. Soc.* **1993**, *115*, 8527.
(27) Roberts, J. E.; Hoffman, B. M.; Rutter, R.; Hager, L. P. *J. Biol. Chem.* **1981**, *256*, 2118.
(28) Roberts, J. E.; Hoffman, B. M.; Rutter, R.; Hager, L. P. *J. Am. Chem. Soc.* **1981**, *103*, 7654.
(29) Benecky, M. J.; Frew, J. E.; Scowen, N.; Jones, P.; Hoffman, B. M. *Biochemistry* **1993**, *32*, 11929.
(30) Hanson, L. K.; Chang, C. K.; Davis, M. S.; Fajer, J. *J. Am. Chem. Soc.* **1981**, *103*, 663.
(31) Fujita, I.; Hanson, L. K.; Walker, F. A.; Fajer, J. *J. Am. Chem. Soc.* **1983**, *105*, 3296.
(32) Du, P.; Axe, F. U.; Loew, G. H.; Canuto, S.; Zerner, M. C. *J. Am. Chem. Soc.* **1991**, *113*, 8614.
(33) Du, P.; Loew, G. H. *Int. J. Quantum Chem.* **1992**, *44*, 251.
(34) Yamamoto, S.; Teraoka, J.; Kashiwagi, H. *J. Chem. Phys.* **1988**, *88*, 303.
(35) Yamamoto, S.; Kashiwagi, H. *Chem. Phys. Lett.* **1988**, *145*, 111.
(36) Dahl, J. P., Avery, J., Eds. *Local Density Approximations in Quantum Chemistry and Solid State Physics*; Plenum Press: New York and London, 1984.
(37) Parr, R. G.; Yang, W. *Density-Functional Theory of Atoms and Molecules*; Oxford University Press: New York, 1989.
(38) Labanowski, J. K., Andzelm, J. W., Eds. *Density Functional Methods in Chemistry*; Springer: New York, Berlin, Heidelberg, 1991.
(39) Sontum, S. F.; Case, D. A. *J. Am. Chem. Soc.* **1985**, *107*, 4013.
(40) Ghosh, A.; Almlöf, J.; Que, Jr., L. *J. Phys. Chem.* **1994**, *98*, 5576.
(41) Antony, J.; Grodzicki, M.; Trautwein, A. X. To be published.
(42) Chen, B. M. L.; Tulinsky, A. *J. Am. Chem. Soc.* **1972**, *94*, 4144.
(43) Binsted, N.; Strange, R. W.; Hasnain, S. S. *Biochemistry* **1992**, *31*, 12117.
(44) Christen, D.; Griffiths, J. H.; Sheridan, J. *Z. Naturforsch.* **1982**, *36a*, 1378.
(45) Ravichandran, K. G.; Boddupalli, S. S.; Hasemann, C. A.; Peterson, J. A.; Deisenhofer, J. *Science* **1993**, *261*, 731.
(46) Grodzicki, M. *J. Phys. B: At. Mol. Phys.* **1980**, *13*, 2683.
(47) Paulsen, H.; Ding, X.-Q.; Grodzicki, M.; Butzlaff, Ch.; Trautwein, A. X.; Hartung, R.; Wieghardt, K. *Chem. Phys.* **1994** *184*, 149.
(48) Paulsen, H.; Kröckel, M.; Grodzicki, M.; Bill, E.; Trautwein, A. X.; Leigh, G. J.; Silver, J. *Inorg. Chem.* **1995**, *34*, 6244.
(49) Zakharieva, O.; Grodzicki, M.; Trautwein, A. X.; Veeger, C.; Rietjens, I. M. C. M. *J. Biol. Inorg. Chem.* **1996**, *1*, 192.
(50) Elbel, S.; Blanck, A.; Walter, H.; Grodzicki, M. *J. Chem. Soc., Faraday Trans. 2* **1985**, *81*, 869.
(51) Elbel, S.; Kudnig, J.; Rünger, G.; Grodzicki, M. *J. Electron Spectrosc. Relat. Phenom.* **1986**, *37*, 329.
(52) Elbel, S.; Grodzicki, M.; Pille, L.; Rünger, G. *J. Mol. Struct.* **1988**, *175*, 441.
(53) To distinguish between the porphyrin $\pi$ MO's $a_{1u}$ or $a_{2u}$ and the $A_{1u}$ radical ($A^{\bullet}_{1u}$) or $A_{2u}$ radical ($A^{\bullet}_{2u}$) states of compound I, in which one of these MO's is oxidized, a lower case a is used for the former and an upper case A for the latter.
(54) Weiss, R.; Mandon, D.; Wolter, T.; Trautwein, A. X.; Müther, M.; Bill, E.; Gold, A.; Jayaraj, K.; Terner, J. *J. Biol. Inorg. Chem.* **1996**, *1*, 377.
(55) Sivaraja, M.; Goodin, D. B.; Smith, M.; Hoffman, B. M. *Science* **1989**, *245*, 738.
(56) Huyett, J. E.; Doan, P. E.; Gurbiel, R.; Houseman, A. L. P.; Sivaraja, M.; Goodin, D. B.; Hoffman, B. M. *J. Am. Chem. Soc.* **1995**, *117*, 9033.
(57) As for the porphyrin radicals, the L.P. radical (L.P$^{\bullet}$) state is denoted by upper case letters.
(58) Bencini, A.; Gatteschi, D. *Electron Paramagnetic Resonance of Exchange Coupled Systems*; Springer-Verlag: Berlin, Heidelberg, 1990.
(59) Noodleman, L. *J. Chem. Phys.* **1981**, *74*, 5737.
(60) The geometry of the porphyrin core with $d$(Fe−N) = 1.97 Å is taken from the crystal structure of iron(II) tetraphenylporphyrin averaged to $D_{4h}$ symmetry. Collman, J. P.; Hoard, J. L.; Kim, N.; Lang, G.; Reed, C. A. *J. Am. Chem. Soc.* **1975**, *97*, 2676.
(61) Grodzicki, M.; Flint, H.; Winkler, H.; Walker, F. A.; Trautwein, A. X. *J. Phys. Chem.*, submitted.
(62) Because of the 4-fold symmetry of the porphyrin core, the value of the rotation angle $\beta = 107.3°$ is equivalent to $\beta = 17.3°$.
(63) Paulsen, H.; Müther, M.; Grodzicki, M.; Trautwein, A. X.; Bill, E. *Bull. Soc. Chim. Fr.* **1996**, *133*, 703.
(64) Müther, M. *Spinkopplung in Modellkomplexen f˙ur Compound I Hämenthaltender Peroxidasen und Katalasen*; PhD thesis, Shaker Verlag: Aachen, 1996.
(65) The geometry of methanol is taken as the gase phase geometry: Callomon, J. H., Hirota, E., Iijima, T., Kuchitsu, K., Lafferty, W. J., Eds. *Landolt-Börnstein. Numerical Data and Functional Relationships in Science and Technology, New Series, Group II: Atomic and Molecular Physics, Volume 15: Structure Data of Free Polyatomic Molecules*; Springer-Verlag: Berlin, Heidelberg, New York, 1987. The iron−oxygen distance is assumed to be 2.1 Å. The angle between iron, oxygen, and carbon is 143.0°, and the tilting angle is chosen as $\alpha = 0°$. Variation of the rotation angle $\beta$ does not change the value of $J$.
(66) Jayaraj, K.; Gold, A.; Austin, R. N.; Ball, L. M.; Terner, J.; Mandon, D.; Weiss, R.; Fischer, J.; DeCian, A.; Müther, M.; Bill, E.; Schünemann, V.; Trautwein, A. X. *J. Am. Chem. Soc.*, submitted.
(67) Patterson, W. R.; Poulos, T. L.; Goodin, D. B. *Biochemistry* **1995**, *34*, 4342.